JOURNAL OF MATERIALS SCIENCE 18 (1983) 766–780

Effect of material parameters on the erosion resistance of brittle materials

S. M. WIEDERHORN, B. J. HOCKEY
National Bureau of Standards, Washington, DC 20234, USA

Erosion data are compared with two theories that have been suggested to explain the erosive behaviour of solids. A dimensional analysis is applied to the variables that are important to erosion, and a multivariate, linear regression analysis is used to fit the data to the dimensional analysis. The results of the linear regression analyses are compared with the two theories in order to evaluate the applicability of these theories to erosion. Although semi-quantitative agreement of the data with the theories is obtained, some discrepancies are apparent. In particular, the dependence of erosion rate on hardness and critical stress intensity factor is greater than predicted by either of the two theories. These discrepancies are attributed primarily to microstructural aspects of erosion that are not modelled by either of the theories.

1. Introduction

Erosion of brittle materials by hard, solid particles is a complex process in which material is lost from the target surface by brittle fracture [1, 2]. The sizes and types of cracks that form in the target surface during impact have been studied extensively and have been shown to depend on several factors: these include particle shape, mass and velocity, and target material hardness and toughness. At low velocities well-developed crack systems form at the impact site: cone cracks are formed by rounded ("blunt") particles [3–5], lateral and medium cracks by angular ("sharp") particles [3, 6–8]. At extremely high velocities the appearance of the impact surface is affected by the ejection of material from the target surface as the particle plows into the surface, and by severe cracking and chipping of the surface after the particle has left the impact site [1, 4, 9, 10]. The types of crack systems that are formed during impact and the conditions that control their formation have been discussed extensively in the references cited above.

Plastic deformation also plays an important role in the erosion process. Thus, a detailed examination of impact sites in brittle materials indicates that a zone of intense plastic deformation forms during contact, beneath the immediate area of the contact [7, 11–13]. Residual stresses associated with the plastic zone force small cracks, known as lateral cracks, to grow from the impact site. Initially, these cracks grow parallel to the target surface, but then curve towards and eventually intersect with the surface resulting in a loss of material from the target. Because of this behaviour, the erosion process in brittle materials is viewed by many investigators as an elastic–plastic event, the plastic deformation at the impact site being the prime driving force for the surface fracture that results in material loss during erosion [1, 2, 10]. While this view of erosion may be over simplified considering the complexity of the process, it has been used to model the erosion process and to develop equations that predict erosion rates as a function of projectile and target parameters that are known to influence the erosion process is brittle materials.

Two elastic-plastic theories have been developed to explain the erosion of brittle solids. Both are based on the assumption that lateral cracks grow in a quasi-static manner as a result of residual stresses introduced by the impact event. In both theories, the size of the lateral cracks, c, are assumed to be determined by the following

 0022–2461/83/030766–15$04.30/0

relation [14]*:

$$P/c^{3/2} = \beta K_c \tag{1}$$

where P is the maximum normal load during impact, K_c is the critical stress intensity factor, and β is a nondimensional constant. The volume of material removed during erosion, V, is determined from the size of the lateral crack, c, and the depth of the crack, d, beneath the target surface

$$V = \pi c^2 d . \tag{2}$$

Since the impact sites are assumed to be non-interacting, the total wear volume, W, is just the summation of the volumes resulting from the individual impact events.

The two elastic-plastic wear theories differ in their assumed dependence of impact load, P, on the kinetic and material parameters that are important to erosion. The theory developed by Evans *et al.* [10] includes dynamic stress wave effects in the calculation of P. A spherical particle is assumed to penetrate into a target without distortion; the contact pressure is assumed to be equal to the dynamic pressure that occurs when the particle first hits the target surface. The depth of penetration is determined from the time of contact and the mean interface velocity, both of which are calculated from a one-dimensional analogue. The final expression for the erosion rate, W, is

$$W \propto v_0^{3.2} R^{3.7} \rho^{1.6} K_c^{-1.3} H^{-0.25} \times [(Z_t Z_p)^{2/3}/(Z_t^{1/2} + Z_p^{1/2})^{8/3}] \tag{3}$$

where v_0 is the initial particle velocity, R and ρ are the particle radius and density, respectively, K_c and H are the target toughness and hardness, respectively, and Z_t and Z_p are the impedances for the target and the particle, respectively, H is the hardness and V_0 is the initial particle velocity. The term within the brackets varies by less than 10% for the materials used in the current study, and therefore will be considered to be a constant for the purpose of this paper. Hence, the equation for the erosion rate reduces to

$$W \propto v_0^{3.2} R^{3.7} \rho^{1.3} H^{-1.25} \tag{4}$$

A quasi-static formulation of the erosion problem is based on work by Wiederhorn and Lawn [15], in which the kinetic energy of the particle is assumed to be absorbed completely by plastic flow when a particle impacts the surface. From this assumption, both the maximum force during contact and the maximum depth of penetration can be calculated. Assuming that the lateral cracks generate at a distance beneath the surface that is equal to the maximum depth of particle penetration, the following equation for the erosion rate is derived [2]

$$W \propto v_0^{2.4} R^{3.7} \rho^{1.2} K_c^{-1.3} H^{0.11} \tag{5}$$

The forms of the two erosion theories presented above are similar in that they express the erosion process by a power law dependence of erosion rate on both particle (v_0, R, ρ) and target (K_c, H) properties. Although the same properties are used in both theories, the exponents for velocity, particle density, and hardness differ. A comparison of these theories with experimental results on erosion indicates that the theories are reasonably consistent with experiment with regard to the exponents for velocity and particle size [2]. The effect of particle density on erosion has not been investigated in any systematic manner, so that there is no way of knowing if the exponents given in Equations 4 and 5 are correct. A study of the effect of hardness, H, and fracture toughness, K_c, on erosion has recently been conducted on a series of ceramics by Evans *et al.* [10] and by Gulden [16]. The data obtained by Evans *et al.* [10] suggest a greater dependence of erosion rate on K_c and H than is predicted by their theory. Aside from these studies, however, there have been no systematic investigations of the effect of K_c and H on the erosion rate of brittle materials.

In this paper, the erosion of dense brittle materials is studied in order to assess the validity of the erosion theories represented by Equations 4 and 5. Of particular interest to this study are the particle velocity and the material parameters K_c and H. The results of our study will show that while both theories provide a qualitative description of the erosion data, neither theory is quantitatively correct. The reason for these differences seems to lie in the simplifying assumptions made

*This relation is concerned with the formation of radial cracks from a sharp indentation. For the relation to be valid, the crack must be large relative to the size of the indentation. The use of this relation to describe lateral crack formation is based on work by Evans *et al.* [10] who showed experimentally that the size of the two cracks were proportional. Hence, the use of Equation 1 to describe erosion phenomenon has its basis in empirical investigations, but has no theoretical justification.

TABLE I Properties of target materials used in erosion study

Material	Young's modulus (GPa)	Hardness (GPa)	Toughness, K_c ($MPam^{1/2}$)	Microstructure
Hot-pressed silicon nitride	317 [17]	19.9 [18]	5.0 [19]	Fully dense ~ 1 μm grain size
Hot-pressed silicon carbide	466 [20]	29.4 [18]	4.0 [21]	Fully dense ~ 1 to 2 μm grain size
Hot-pressed aluminium oxide	425 [22]	22.0 [18]	4.0 [23]	Fully dense ~ 3 to 4 μm grain size
Sintered aluminium oxide	425 [22]	21.7 [18]	2.2 [24]	Fully dense ~ 30 μm grain size
Sapphire	425 [22]	21.7 [18]	2.2 [24]	Single crystal $\{10\bar{1}1\}$ plane
Silicon	168 [25]	10.6 [18]	0.7 [26]	Single crystal $\{112\}$ plane
Silica glass	75 [27]	8.7 [18]	0.77 [28]	C7940
Soda-lime–silica glass	75 [27]	6.3 [18]	0.75 [28]	C0800
Magnesium oxide	330 [22]	8.0 [29]	2.6 [18]	Fully dense ~ 10 to 15 μm grain size

in both theories of erosion. As will become apparent, details of the microstructure and material interaction during impact affect erosion in ways not fully accounted for by the present models of erosion.

2. Experimental procedure

The target materials used in the present investigation provided a reasonably wide range of target properties (K_c and H) and microstructure for study (Table I). Examination of the impact area by transmission electron microscopy showed that all of the materials selected for investigation deformed plastically when subjected to impact [13]*. The cracks that were generated by the impacting particles, while originating from within the deformed zone, exhibited no evidence of localized plastic deformation at the crack tip, and accordingly propagated in a brittle manner†. Therefore, these materials fit within the framework of the theories discussed above.

The particles used for erosion measurements were 150 μm SiC abrasive grains. Because of the hardness of these particles it was felt that they simulated the hard, non-yielding particles assumed to be responsible for erosion in the theories used to derive Equations 4 and 5. To achieve a uniform particle size for investigation, all particles were sieved between an 80 and 120 mesh screen before being used in erosion investigations. The particles that were used passed through the 80 mesh screen, but were retained by the 120 mesh screen.

The erosion apparatus used in this study has been described previously [30]. Briefly, the equipment was desgined to feed abrasive particles into a high velocity air stream, which propelled the particles against the specimen surface (Fig. 1). The particles were accelerated by passing them through a tungsten carbide nozzle ~ 5 cm long and 0.16 cm in internal diameter. The acceleration of the particles to high velocity is accomplished within the nozzle. The particle–air mixture is passed through a ceramic tube, 2 cm in diameter, to obtain a relatively uniform beam of abrasive particles. High temperatures can be achieved by feeding a propane–oxygen mixture through a ring-burner into the top of the ceramic tube. The high velocity particle–air

*The technique of transmission electron microscopy was applied only to the crystalline materials used in this investigation. With regard to their deformation and fracture properties, however, other studies suggest that the behaviour of glass is similar to that of crystalline materials (see Lawn *et al.* [13] for a discussion of this point).

†With the exception of MgO for which dislocations can probably be generated at crack tips.

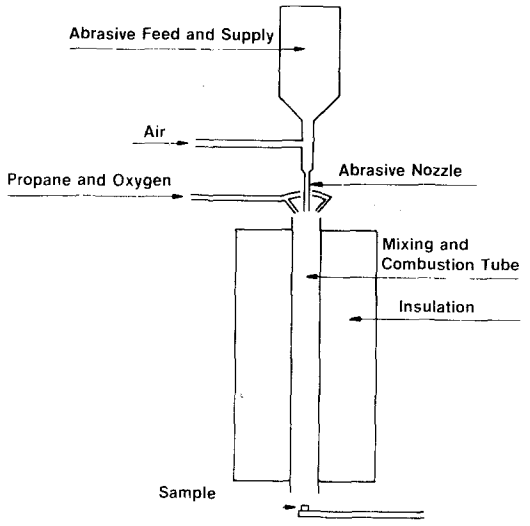

Figure 1 Schematic diagram of erosion equipment (after Wiederhorn and Roberts [30]).

stream sucks the flame from the burner into the ceramic tube to produce temperatures as high as 1200° C.

The particle velocities were measured by using a time-of-flight technique developed originally by Ruff and Ives [31]. In this technique, two discs rotate on a common axis which is parallel to the direction of the erosive gas stream. The disc closest to the exit port of the erosion apparatus contains a slit, which permits particles to pass through the disc and impinge on the second disc. For a fixed rotational speed, the position of the erosion mark on the second disc, relative to the position of the slit on the first disc, establishes the particle velocity.

The sensitivity of the double disc technique to measure particle velocities was improved during the course of the present study by mounting partially silvered glass microscope slides on the second disc directly below the slit on the first disc [32]. Particles that impinged on the glass slide formed impact damage that destroyed the reflectivity of the microscope slide in the immediate area of impact. As a consequence, the position of the erosion marks on the microscope slides were easily observed and measured. Quantitative optical microscopy was used to improve the accuracy of measuring the position of the erosion marks on the microscope slides. The original technique was further improved by first rotating the disc in one direction to obtain an erosion mark and then in the opposite direction to obtain a second erosion mark. This procedure doubled the distance between marks, thus improving the accuracy of the velocity measurements.

The specimens used in this study were ~ 1.25 cm square plates approximately 0.6 cm thick. They were mounted on a support arm and held with their wide face normal to the stream of erosive particles. Specimens were exposed to a fixed mass of erosion particles, which ranged from 25 to 400 g depending on the target material and the particle velocity selected for study. The mass lost by the target during each experiment was measured to at least 1% accuracy using an analytical balance. The erosion rate was calculated from the fraction of particles that intersected the specimen. The number of particles impacting the target was estimated from the mass of abrasive used and the mean particle size of the abrasive (approximating the particles as spheres). Finally, the volume loss per particle impact (i.e. the erosion rate) was calculated from the mass lost from the specimen per particle impact, and the target density.

3. Results

The results of our studies are shown in Figs. 2 to 4*. In each case the log of the erosion rate (expressed as volume lost per particle impact) is plotted against the log of the particle velocity. Fig. 2 presents the results obtained at room temperature. The erosion rate was measured for velocities ranging from 37 to 94 m sec^{-1}, for the nine target materials used in the present study. The erosion data shown in Fig. 2 fit a power law function as expressed by Equations 4 and 5. The slopes of the curves at room temperature ranged from 1.9 for hot-pressed silicon carbide to 2.9 for silicon and silica glass. The standard error of the slopes ranged from ~ 0.003 to ~ 0.25 with a mean value of ~ 0.1 (Table II), which indicates that at the 95% confidence level and for two degrees of freedom, a difference in slope of ~ 0.4 is significant. With the exception of the hot-pressed silicon nitride, the values of these slopes are similar to those reported by other investigators on similar materials [33–38]. The slope of the hot-pressed silicon nitride was about one-half that reported earlier by Gulden [16]. The erosion rate of the target materials shown in Fig. 2 decreases as the tough-

*The data used in these figures are summarized in Appendix B.

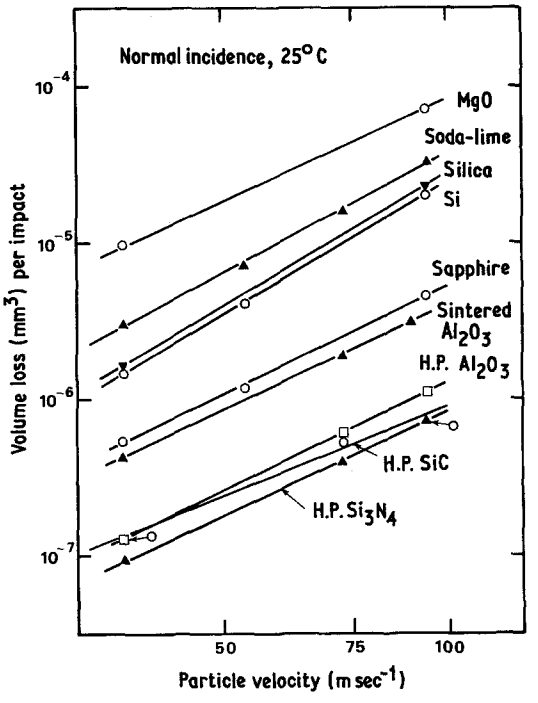

Figure 2 Erosion of brittle materials at 25° C, normal incidence impact, 150 μm SiC particles. For clarity the errors given in Table IB have been left off the figure.

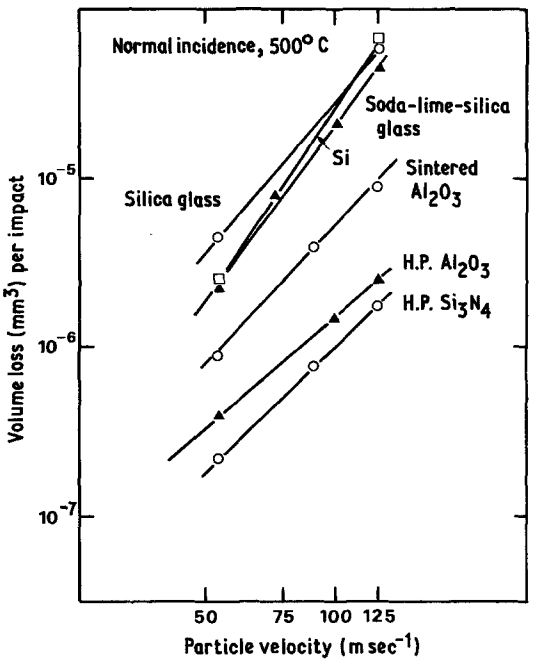

Figure 3 Erosion of brittle materials at 500° C, normal incidence impact, 150 μm SiC particles. For clarity the errors given in Table IB have been left off the figure.

ness of the target material increases, a finding that provides qualitative support for the erosion theories described by Equations 4 and 5. A quantitative comparison of the two theories with the data will be made in a later section of this paper.

The erosive wear data collected at 500 and 1000° C are shown in Figs. 3 and 4, respectively, for several of the target materials used in the present study. The data shown in these figures are similar to those obtained at room temperature. However, for some of the materials the slopes of the curves at elevated temperatures were significantly greater than those obtained at room temperature. Although the relative position of the erosion curves on the graph was roughly the same at elevated temperature and room temperature, small systematic differences in erosion behaviour were obtained for some of the materials. Thus, elevated temperatures appeared to slightly enhance the erosion rate of silicon, and hot-pressed silicon nitride at the higher velocities, whereas the erosion rate of glass, sapphire, and sintered aluminium oxide was reduced at the lower velocities. The results of the present study were similar to those reported earlier by the present authors on a smaller set of data [7].

4. Discussion

The purpose of this paper is to present data that can be compared with the elastic-plastic theories (Equations 4 and 5) that have been developed to explain the erosion of brittle materials. In particular the erosion data were used to evaluate the exponents of v_0, K_c, and H, which were then compared with those given in Equations 4 and 5. Since K_c and H are determined by the properties of the target material, they cannot be varied independently, and hence have to be compared with the theories in combined form: $K_c^{-1.3}H^{-0.25}$ for Equation 4; $K_c^{-1.3}H^{0.11}$ for Equation 5. A second way of comparing the exponents of Equations 4 and 5 with the experimental data is by first expressing these two equations in dimensionless form through the use of a dimensional analysis and then fitting the dimensionless equation to the experimental data to obtain the exponents. Both of these techniques will be used in this paper.

4.1. Velocity exponents

The velocity exponents obtained in this paper are summarized in Table II, and can be compared with other data reported in the literature for similar materials (Table III). As can be seen from these tables, data obtained in the present

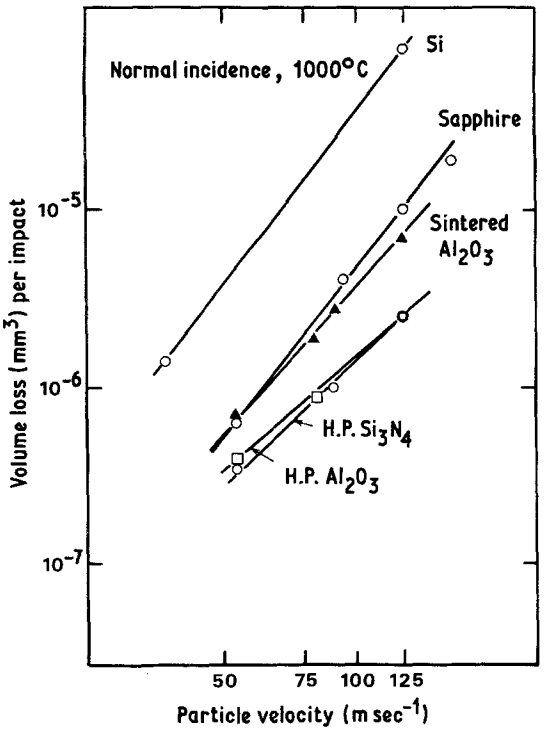

Figure 4 Erosion of brittle materials at 1000° C, normal incidence impact, 150 μm SiC particles. For clarity the errors given in Table IB have been left off the figure.

study are reasonably consistent with those reported by other authors. Most of the differences between the results shown in Tables II and III are believed to be due to small, systematic, interlaboratory differences in experimental technique. The results on hot-pressed silicon nitride, however, differ significantly from our own because of the large difference in velocity exponent (4 versus 2.2) obtained in the two studies.

The velocity exponents from Table II cluster more closely about the value (2.4) predicted by the quasi-static model of erosion, Equation 5, than the value (3.2) predicted by the dynamic model of erosion, Equation 4. This conclusion has to be tempered by the fact that the velocity exponent of v increases as the temperature is increased and tends to fall between the two predicted values. Furthermore, recent studies on silicon by Scattergood and Routbort [36] suggest that the velocity exponent increases as the particle size decreases. Hence, for small particles, the trend is toward better agreement between the dynamic theory of erosion and experimental measurement. These dependences of velocity exponent on temperature and on particle size are not predicted by either theory.

4.2. Target parameters

The erosion data presented in Fig. 2 are compared with the material parameters H and K_c in Fig. 5. Fig. 5a compares the erosion data with the dynamic theory of erosion; Fig. 5b compares the erosion data with the quasi-static theory of erosion. With the exception of MgO, the data on both figures plot as straight lines, lending credence to the suggested theories of erosion. However, both sets of data are represented by lines with slopes greater than 1, the theoretically expected slope. The empirical slope for the dynamic erosion theory, ~ 1.2, is closer to the expected slope of 1 than is the slope, ~ 1.5, for the quasi-static theory of

TABLE II Velocity exponents for erosion data: normal incidence

Material	Temperature 25° C	500° C	1000° C
Magnesium oxide, polycrystalline	2.2	–	–
Soda-lime–silica glass	2.5 (0.12)*	3.5 (0.20)	–
Vitreous silica	2.9	3.0	–
Sapphire	2.3 (0.10)	2.4 (0.25)	3.3 (0.03)
Sintered aluminium oxide, 30 μm	2.3 (0.003)	2.8 (0.09)	2.7 (0.15)
Hot-pressed aluminium oxide, 3 to 4 μm	2.3 (0.03)	2.1 (0.04)	2.3 (0.11)
Silicon	2.9 (0.03)	3.8	3.4
Hot-pressed silicon carbide	1.8 (0.16)	–	–
Hot-pressed silicon nitride	2.1 (0.08)	2.5 (0.03)	2.4 (0.20)

*The numbers in parentheses give the standard error for the value of the velocity exponent, which was determined by a linear regression analysis of the mean wear values given in Table IB. For exponents that were determined from only two wear values, no standard error is given.

TABLE III Velocity exponents for erosion data: normal incidence

Target material	Erosion particles	Exponent	Reference
Soda-lime–silica glass	SiC, 120 grit	3.0	[33]
MgO (96.5%)	SiC, 120 grit	2.7	[33]
Al_2O_3 (99.5%)	SiC, 120 grit	2.6	[33]
Pyrex glass	Al_2O_3 30 μm 10 μm	2.2 2.7	[34]
Hot-pressed Si_3N_4	SiC 8 to 940 μm	4.0	[35]
Silicon	Al_2O_3 23 μm to 270 μm	3.4 to 2.6 depending on particle size	[36]
Reaction bonded SiC	Al_2O_3 130 μm 270 μm	2.3 2.0	[37]
Hot-pressed SiC	Al_2O_3 130 μm 270 μm	1.8 1.5	[38]

erosion. Similar values of slopes were observed by Gulden [16] in an erosion study on a different set of materials. Hence, from this type of analysis, the dynamic theory of erosion appears to provide a somewhat better fit to the erosion data than does the quasi-static theory.

The data for MgO are not consistent with the data obtained for the other materials, undoubtedly because of the type of impact damage formed in the surface of this material. The MgO cracked along the grain boundaries in the vicinity of the impact site, so that each impact event formed a loosely connected aggregate of grains that surrounded the impact site. These damaged areas were easily removed from the surface during erosion, resulting in a higher rate of erosion than predicted theoretically. In essence, the mechanism of erosion for MgO differed markedly from that for other materials. Erosion of polycrystalline MgO probably does not fit the lateral chipping models.

4.3. Dimensional analysis

Dimensional analysis [39] is an alternative method of obtaining relationships between the parameters that affect erosion. While not providing a specific

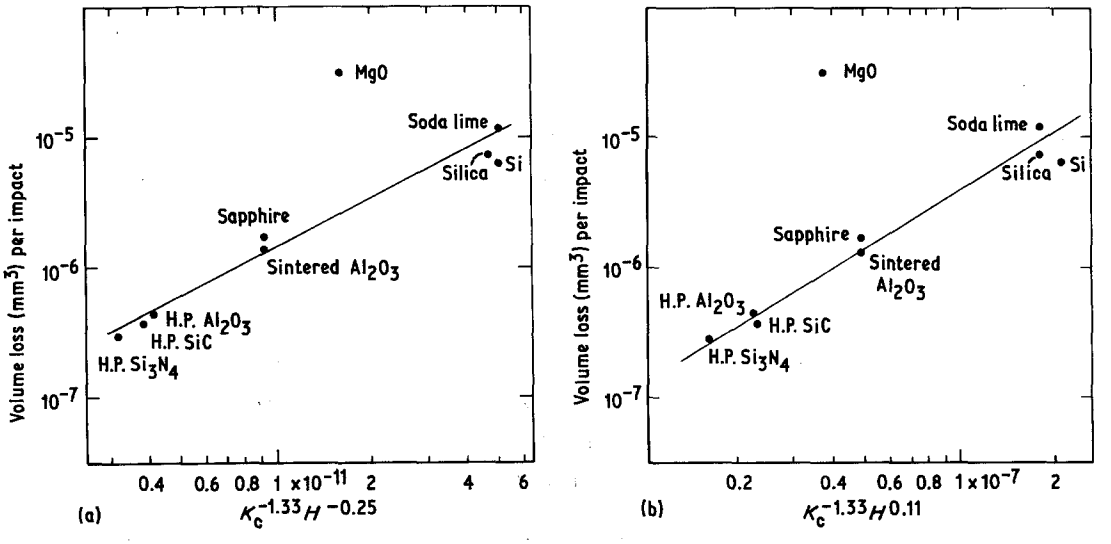

Figure 5 Comparison of the erosion data with the theories given by (a) Equation 4 [10] and (b) Equation 5 [2]. The volume lost per particle impact was selected from Fig. 2 at a velocity of 63 m sec^{-1}. Units of hardness and toughness used to calculate the abscissae of this figure were Pa and $Pam^{1/2}$, respectively.

model of erosion, dimensional analysis provides an operative equation to describe erosion in terms of dimensionless groups of variables and empirical constants determined from a regression analysis of experimental data. The empirical constants can be compared with those determined from the two erosion models to yield an unbiased comparison of theory and experiment.

To apply dimensional analysis, we assume that the parameters that control erosion are those given in Equations 4 and 5. The volume loss per particle impact, W, is then a function of these parameters:

$$W = F(v_0, R, \rho, K_c, H) \tag{6}$$

Using the standard methods of dimensional analysis [39], the following functional relation is obtained:

$$W/R^3 = A(K_c^2/RH^2)^a(\rho\, v^2/H)^b \tag{7}$$

where A is a dimensionless constant*.

Because Young's modulus has been suggested as a variable that contributes to crack formation during hardness indentations [40], the treatment given above was extended to include Young's modulus, E. The equation obtained is similar to Equation 7, but contains an extra dimensionless term, E/H

$$W/R^3 = A'(K_c^2/RH^2)^a\,(\rho\, v^2/H)^b\,(E/H)^c \tag{8}$$

Equation 7 contains three dimensionless groups each of which has physical meaning. The first represents the ratio of the volume loss during impact to the volume of the impacting particle. All other parameters being constant, the erosion rate will increase as the particle volume (i.e. particle size) increases. The second group (K_c^2/RH^2) can be represented as the ratio of the inverse of target brittleness to the size of the impacting particle. This interpretation follows from the fact that $(K_c/H)^2$ is a measure of the relative resistance of a target to fracture during an impact event: the higher the value of $(K_c/H)^2$, the more resistant the target will be to fracture. The parameter $(K_c/H)^2$ can be thought of as representing a critical scaling dimension above which fracture occurs during contact. The inverse quantity, $(H/K_c)^2$, is a useful index of "brittleness". [40] The third group, $(\rho v^2/H)$ represents the ratio of the particle energy density, i.e. kinetic energy per particle volume, ρv^2, to the hardness, which can be considered as a deformation energy density. The fourth dimensionless constant in Equation 8 can be considered as the ratio of the elastic to the plastic energy density.

The constants a and b for the dynamic model of erosion, have values of -0.67 and 1.58, respectively. For the quasi-static erosion model, the values of a and b are -0.67 and 1.22, respectively. The value of c in Equation 8 is zero for both models. Hence, the two models differ only in the exponent of the third dimensionless group.

Empirical values of the constants, a, b and c for Equation 7 and 8 were obtained by a multiple regression analysis of the data (MgO excluded) reported in Fig. 2. The results of the analysis are given in Table IV. The statistics in this table give useful information on the relative importance of the constants a, b and c with regard to the fit of the erosion data. Virtually the same values of a and b and their standard errors are obtained regardless of whether two or three independent variables are used for the regression analysis. The standard errors for a and b are relatively small (7 and 11% of the mean, respectively) and the values of t† computed for these constants are large and hence significant for any reasonable level of probability. By contrast, the standard error for c (55% of the mean) is large, and the value of t obtained for this constant is not significant at the 95% level, which suggests that the value of c reported in Table IV does not differ significantly from zero. From this discussion we conclude from our results that the wear rate does not depend in any significant way on the ratio of the Young's modulus to the hardness, E/H‡. This conclusion is supported by the fact that r^2, which gives the fraction of the variance accounted for by the regression analysis, only changes from 94 to 95% when E/H is added as an independent variable. Consequently, the values of a and b determined from the two parameter regression analysis will be used for purposes of further discussion in this paper.

As can be seen from Table IV, the empirical value for a, -0.932, is greater in absolute value

*This equation is derived in Appendix A.

†For a definition of t, see any standard statistics text, e.g. [41].

‡This conclusion must be tempered by the fact that E/H only varied by a factor of about 2 in the present study. A larger variation of this parameter might indicate a significant dependence of wear on E/H.

TABLE IV Determination of the exponents of Equations 7 and 8 by a multivariable regression analysis (room temperature data)

Exponent	Regression coefficient	Standard error of coefficient	Computed t
Equation 7			
a	−0.932	0.110	− 8.44
b	1.384	0.093	14.92
Intercept, ln A		−11.40	
Multiple correlation		0.971	
r^2		0.942	
Standard error of estimate		0.415	
Equation 8			
a	−0.905	0.106	− 8.56
b	1.312	0.096	13.66
c	−0.669	0.364	− 1.84
Intercept, ln A		− 9.84	
Multiple correlation		0.975	
r^2		0.950	
Standard error of estimate		0.415	

than the theoretical value of a, −0.667, given by Equations 4 and 5. The value for b, 1.38, lies approximately half-way between the value of 1.22 predicted by the quasi-static theory and the value of 1.58 predicted by the dynamic theory. Using the values of a and b from the multiple regression analysis, Equation 8 can be expressed in a form that is similar to that of Equations 4 and 5

$$W \propto v^{2.8} R^{3.9} \rho^{1.4} K_c^{-1.9} H^{0.48} \quad (9)$$

The most significant difference between Equations 4 and 5 and Equation 9 is the dependence of the wear rate on the fracture toughness and the hardness. The exponent of K_c suggests a stronger dependence on this value than is predicted theoretically. As K_c of the target is increased, the difficulty of removing material by chipping increases more rapidly than predicted by either theoretical treatment. Possible sources of this variation involve the effect of microstructure on erosion and the random nature of the impact process. These sources of variation imply that the models suggested to explain erosion may be too simple to account fully for the effect of fracture toughness on the erosion rate. The effect is microstructure and the random nature of the particle impact process will be discussed more fully in a later section of this paper.

In view of the fact that most theories of erosion predict a decrease in the erosion rate as the hardness in increased, the positive exponent of the hardness in Equation 9 requires some rationalization. An explanation for the positive exponent for hardness in Equation 9 can be developed from a closer examination of the quasi-static theory of erosion. In this theory, hardness determines both the depth of penetration and the maximum load during impact. In the expression for maximum load, hardness enters the equations with a positive exponent, such that for a fixed impact energy the maximum impact load increased as the hardness is increased. Since the amount of chipping is proportional to the maximum load during impact, the relation between load and hardness suggests that the erosion rate increases as the hardness increases. Penetration is also important because it determines the depth beneath the surface where lateral cracks form: the deeper the penetration (lower hardness) the greater the erosion rate. In the final erosion equation, the pentration term and the load term oppose one another with regard to hardness and the larger of the two determines the exponent for the hardness. In Equation 5 the load term dominates, and the exponent for the hardness is positive. Using this same line of reasoning, the results of the regression analysis suggest that hardness effects surface load to a greater extent than penetration depth, resulting in a positive exponent for hardness in Equation 9. The fact that the exponent in Equation 9 is greater than 0.11 suggests that the effect of the surface load term on erosion is greater than that predicted by the quasi-static theory of erosion.

4.4. Microstructural analysis of impact damage

As noted in the previous section of this paper, the large exponent of K_c in Equation 9 may have its origin in effects due either to target microstructure or to the random nature of the particle impact process. The two theories of erosion discussed in this paper are predicated on the assumption that the particles impact on sharp corners and that the type of damage is similar, regardless of the properties of the target material. If either assumption is not valid, then the dependence of erosion on K_c will differ from that given by Equations 4 and 5.

Examination of surfaces that have been impacted by small numbers of particles yields information on both the type of damage that occurs during erosion and the relative number of particles that result in chipping from the target surface. When particles impact the target, they either leave shallow, plastic impressions, or small chipped regions at the point of impact (Fig. 6). The plastic impressions are probably left by particles that were not oriented to impact on a sharp corner, but on a side, or edge. The residual plastic impressions in the target surface suggest that the deformation was not concentrated sufficiently to nucleate and propagate surface cracks, i.e. stresses at the impact site did not exceed the threshold for fracture at these shallow impressions. Consequently, only a fraction of particles that impact the target surface are effective in the removal of material. If this fraction depends on K_c, then the erosion of the target will also depend on K_c, but in a way not given by Equations 4 and 5.

In our study of the morphology of eroded surfaces we have observed that as the toughness of the material is increased, the relative number of impacts that result in chipping is reduced, regardless of impact velocity. This observation of impact behaviour is illustrated in Fig. 6, where erosion surfaces of glass, sapphire, and silicon nitride are compared. As can be seen, the fraction of impacts that results in fracture and material removal increases as the fracture toughness of the target decreases. For glass, every impact site in Fig. 6a has resulted in crack formation. By contrast, both the sapphire and the silicon nitride have several impact sites where plastic impressions were left, but where crack formation was not apparent. This observation suggests that the functional dependence of erosion rate on K_c for brittle materials is not completely described by either theoretical treatment of erosion (Equations 4 and 5), but instead depends on factors that are related to the nucleation of cracks at the impact site. Apparently crack nucleation is relatively easier when a "blunt" impact occurs in glass or silicon, than when it occurs in the hot-pressed materials used in the present study. Hence, the rather large dependence

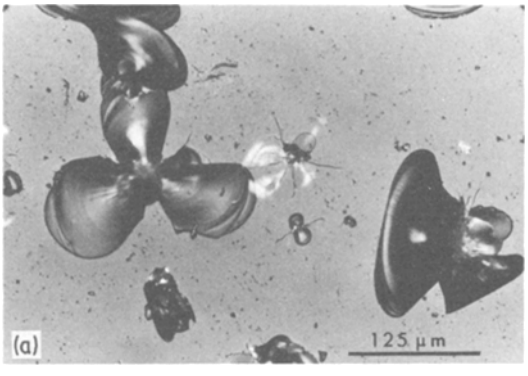

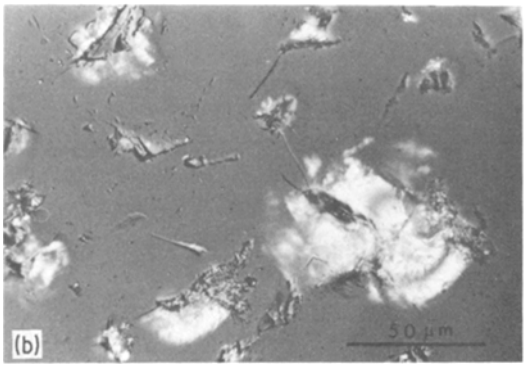

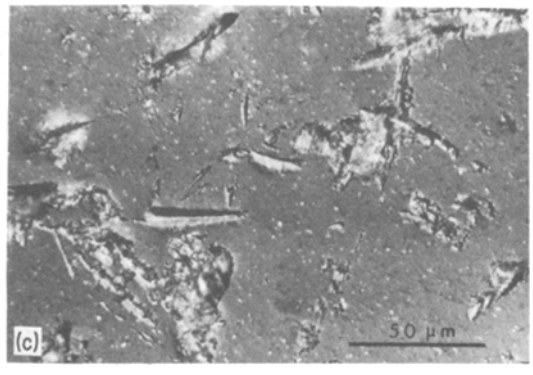

Figure 6 Single particle impact damage in ceramic materials. Optical micrographs of (a) soda-lime–silica glass, 90 m sec^{-1}; (b) sapphire, 90 m sec^{-1}; (c) hot-pressed silicon nitride, 90 m sec^{-1}.

of erosion rate on K_c and H reported in this paper can be attributed in part to statistical effects of particle orientation during erosion and the ease with which cracks nucleate in the target surface.

A second possible explanation for the observation of a larger than expected dependence of erosion rate on K_c and H has to do with the geometry of the cracks that form during the erosion process. The theories that have been proposed to explain erosion assume that cracks propagate from the impact site in a self-similar fashion, i.e. the cracks formed during impact are geometrically similar. Once nucleated, the cracks are assumed to propagate to the target surface. Thus, material is removed from the target by each impact. In contrast to these expectations, microscopic examination of the target surface indicates that the effectiveness of material removal from the target seems to depend on the fracture toughness of the target. Thus for the hot-pressed materials used in this study, cracks are often observed to arrest within the solid Fig. 7b and c so that cracking during impact does not result in material loss. A second or third impact in the vicinity of the primary impact site is needed for material to be removed from the target. In contrast to this behaviour, complete chipping from the primary impact site is a more frequent occurrence for the more brittle materials such as silicon or glass (Fig. 7a). Thus, as the fracture toughness of the material increases, the efficiency of material removal per impact event is less than predicted theoretically, and the effect of K_c on the erosion rate is greater than predicted theoretically.

Before turning from the subject of microstructure, it is worth commenting on the erosion results obtained for aluminium oxide and sapphire. As can be seen from Fig. 2, the erosion rates of sapphire and sintered aluminium oxide are approximately three times that of the hot-pressed aluminium oxide. The difference in behaviour of the two polycrystalline materials is attributable to the difference in grain size of the two materials. The grain size, 3 to 4 μm, of the hot-pressed material was considerably smaller than the size of the lateral cracks that were formed upon impact. As a consequence, lateral cracks interact with many grains during propagation, and the effective value of K_c resisting the growth of lateral cracks is that typical of polycrystalline aluminium oxide, $\sim 4\,\mathrm{MPam}^{1/2}$. By contrast, lateral cracks formed in the sintered aluminium oxide, grain size ~ 30 μm, are usually contained within a single grain, and the effective K_c resisting crack growth is more typical of values obtained from single crystal fracture measurements, $\sim 2\,\mathrm{MPam}^{1/2}$.

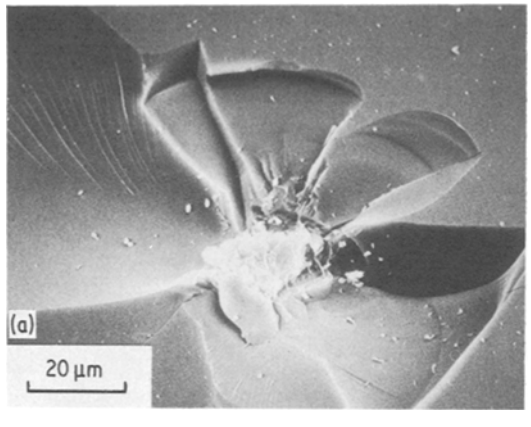

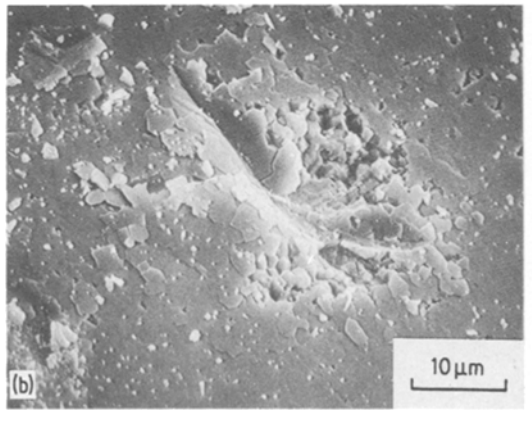

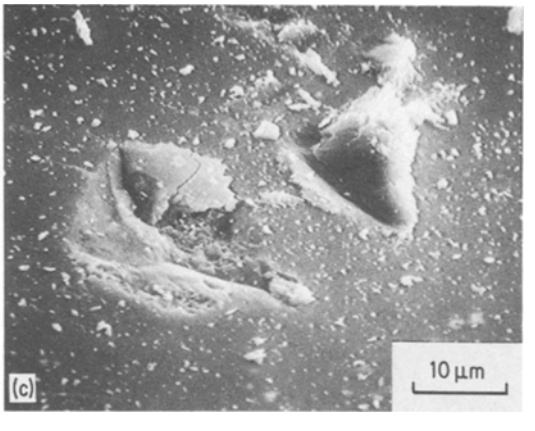

Figure 7 Single particle impact damage in ceramic materials. Scanning electron micrographs of (a) soda-lime–silica glass, 54 m sec^{-1}; (b) hot-pressed aluminium oxide, 90 m sec^{-1}; (c) hot-pressed silicon nitride, 90 m sec^{-1}.

Using Equation 9, the erosion rate for the large grain aluminium oxide should be approximately 3.7 times that obtained for the fine grained aluminium oxide. In Fig. 2, the erosion rate for the sintered aluminium oxide is approximately 3.3 times that of the hot-pressed material, which is close to the expected value. The fact that the erosion rate of the sintered aluminium oxide is close to that obtained for sapphire lends further support for this interpretation of the data.

4.5. Erosion at elevated temperatures

As can be seen by comparing Figs. 3 and 4 with Fig. 2, the temperatures employed in the present study have a marginal effect on the rate of erosion. This finding is consistent with that reported earlier by the authors from a more limited set of data collected on some of the same materials studied in this paper [7]. Since dislocation mobility is enhanced by increasing the temperature, it was expected that both the hardness and fracture toughness, and hence the erosion rate, would be modified by increasing the temperature. Indeed, when loads are applied slowly, both the hardness and toughness of ceramic materials are strongly dependent on temperature [19, 26, 29, 42, 43]. The fact that significant changes in the erosion behaviour are not observed at elevated temperatures suggests that for conditions of dynamic loading, both the hardness and the toughness are invariant with temperature. This supposition is supported by dynamic toughness measurements on hot-pressed silicon nitride [44, 45], and by the fact that cracks are observed to form in soda-lime–silica glass at temperatures above the softening point of this glass [46, 47].

Although temperature does not play a dominant role in the erosion of ceramics under the conditions used in the paper, minor differences between low and elevated temperature behaviour can be attributed to plastic flow. Because lateral cracks form after the impact event and are driven by residual stresses at the impact site, relaxation of those stresses or modification of the resistance of the target to crack growth as a result of plastic deformation can alter the size of chips that are formed after impact. Such effects are feasible when the relaxation time of the material for plastic flow is less than the time required for the lateral cracks to complete their growth. In an earlier study on soda-lime–silica glass at 500° C, the temperature dependence of the erosion rate was attributed to such plastic relaxation [46]. In the present study, the small differences between low and elevated temperature behaviour may also be attributable to the same types of processes.

Acknowledgements

The authors gratefully acknowledge the support of the Office of Naval Research, Metallurgy and Ceramics Program. Helpful discussions with B. R. Lawn are also gratefully acknowledged.

Appendix A:
Dimensionless erosion equation

This Appendix is written for those readers who are unfamiliar with the technique of dimensional analysis. A concise description of the technique can be found from Kay and Nedderman [48]. The procedure outlined in this reference is followed here.

Starting with Equation 6, we assume that the wear rate can be expressed as a power series expansion of the parameters v_0, R, ρ, K_c and H:

$$W = \sum_i \alpha_i (v_0^{a_i}, R^{b_i}, \rho^{c_i}, K_c^{d_i}, H^{e_i}) \quad \text{(A1)}$$

α_i being a dimensionless coefficient for each term. of the senes. The dimensions of each term in the expansion must equal the dimensions of W in order for Equation A1 to be dimensionally consistent.

When the dimensions are substituted for the parameters in Equation A1, each term in the expansion must have the following dimensional form:

$$L^3 = (L/T)^{a_i} L^{b_i} (M/L^3)^{c_i} (M/T^2 L^{1/2})^{d_i} (M/T^2 L)^{e_i} \quad \text{(A2)}$$

where L, T, and M represent the dimensions of length, time, and mass.

Equating the exponents for each dimension we obtain three simultaneous equations in terms of the exponents a_i, b_i, c_i, d_i, and e_i. If two of the unknowns are selected as independent variables, the other unknowns can be expressed in terms of these two variables. For example, if c_i and d_i are selected then the following equations are obtained for a_i, b_i, and e_i:

$$\begin{aligned} a_i &= -3 - 2c_i \\ b_i &= 3 - d_i/2 \\ e_i &= -c_i - d_i \end{aligned} \quad \text{(A3)}$$

If these are substituted into Equation A1, the

following expression is obtained for the wear rate W:

$$W/R^3 = \sum_i \alpha_i (v^2\rho/H)^{c_i} (K_c^2/RH^2)^{d_i/2} \quad \text{(A4)}$$

Since the two theories developed to explain erosion are power functions of the variables given in Equation A4, only one term in the series need be retained in order to compare the dimensional analysis with the theoretical expressions given by Equations 4 and 5. Hence, the following relation is obtained for the erosion rate:

$$W/R^3 = A (K_c^2/RH^2)^a (\rho v^2/H)^b \quad \text{(A5)}$$

where A is a dimensionless constant and the exponents of Equation A4 have been written as a and b. Equation A5 is identical to Equation 7 of the text. As noted earlier, the undetermined constants a and b are evaluated by an empirical fit of erosion data.

Equation A5 is not a unique dimensionless representation of the parameters that control erosion. For example, if b_i and c_i had been selected as the independent constants, then the following erosion equation would have been obtained

$$W(H/K_c)^6 = A'(v^2\rho/H)^c (RH^2/K_c^2)^b \quad \text{(A6)}$$

Equations A5 and A6 can be shown to be equivalent by dividing both sides of the equation by $(RH^2/K_c^2)^3$. By systematically solving for all possible combinations of the exponents in Equation A1, five variants of Equation A5 were found. These could all be reduced to Equation A5 by judicial manipulation (multiplying or dividing) of the dimensionless parameters K_c^2/RH^2 and $\rho v^2/H$.

There is a certain arbitrariness in selecting one of the dimensionless equations for a comparison with the experimental data. We justify the selection of Equation A5 on the basis of its simple form and the ease with which the dimensionless variables K_c^2/RH^2 and $\rho v^2/H$ can be given physical interpretation. Furthermore, this arrangement of the variables in Equation A5 separates the variants used in the present study more effectively than the others, and permits us to compare the theoretical equations with the results of the dimensional analysis more readily. Regardless of which form of the dimensionless analysis is used, one can show that they are all equivalent, provided the error is minimized in the term containing the wear rate, i.e. W/R^3. This equivalence can be demonstrated by using the basic equations for a multiple regression analysis [41].

Appendix B

TABLE IB Summary of erosion data

Material	Temperature (° C)	Particle velocity (m sec^{-1})	Erosion rate (mm^3)
Hot-pressed Si_3N_4	25	94	7.4×10^{-7} (0.8)*
		73	4.0×10^{-7} (0.6)
		37	9.9×10^{-8} (2.6)
	500	125	1.8×10^{-6} (0.2)
		90	8.1×10^{-7} (2.0)
		54	2.2×10^{-7} (0.4)
	1000	125	2.5×10^{-6} (0.2)
		90	9.9×10^{-7} (0.5)
Hot-pressed SiC	25	94	7.2×10^{-7} (1.5)
		73	5.3×10^{-7} (0.2)
		37	1.4×10^{-7} (0.3)
Hot-pressed Al_2O_3	25	94	1.1×10^{-6} (0.2)
		73	6.0×10^{-7} (0.6)
		37	1.3×10^{-7} (0.4)
	500	125	2.5×10^{-6} (0.1)
		100	1.5×10^{-6} (0.1)
		54	4.1×10^{-7} (0.1)
	1000	125	2.5×10^{-6} (0.1)
		81	8.7×10^{-7} (0.6)
		54	3.8×10^{-7} (0.4)

TABLE IB continued

Material	Temperature (° C)	Particle velocity (m sec^{-1})	Erosion rate (mm^3)
Sintered Al_2O_3	25	90	3.2×10^{-6} (0.4)
		73	2.0×10^{-6} (0.1)
		37	4.3×10^{-7} (1.3)
	500	125	9.1×10^{-6} (1.0)
		90	3.9×10^{-6} (1.1)
		54	8.8×10^{-7} (3.6)
Sintered Al_2O_3	1000	125	6.7×10^{-6} (2.1)
		90	2.8×10^{-6} (0.7)
		81	1.8×10^{-6} (0.6)
		54	7.0×10^{-7} (2.5)
Sapphire	25	94	4.6×10^{-6} (0.4)
		54	1.2×10^{-6} (0.1)
		37	5.5×10^{-7} (0.1)
	500	125	9.1×10^{-6} (1.0)
		90	3.9×10^{-6} (1.1)
		54	8.8×10^{-7} (3.6)
	1000	125	9.8×10^{-6} (0.7)
		94	3.8×10^{-6} (0.3)
		54	6.4×10^{-7} (0.6)
Silicon	25	94	2.1×10^{-5} (0.1)
		54	4.1×10^{-6} (0.3)
		37	1.4×10^{-6} (0.1)
	500	125	6.5×10^{-5} (0.7)
		54	2.6×10^{-6} (0.2)
	1000	125	7.7×10^{-5} (1.0)
		54	4.6×10^{-6} (0.7)
Sintered MgO	25	94	7.3×10^{-5} (0.7)
		37	9.8×10^{-6} (0.2)
Fused Silica	25	94	2.3×10^{-5} (0.3)
		37	1.6×10^{-6} (0.2)
	500	125	6.0×10^{-5} (0.5)
		54	4.7×10^{-6} (0.0)
Soda-lime–silica glass	25	94	3.2×10^{-5} (0.7)
		73	1.7×10^{-5} (0.4)
		54	7.1×10^{-6} (0.7)
		37	3.2×10^{-6} (0.7)
	500	125	4.4×10^{-5} (1.2)
		100	2.2×10^{-5} (0.6)
		73	8.3×10^{-6} (0.4)
		54	2.3×10^{-6} (0.5)

*The numbers in parentheses are the standard deviation of each fit. Two to ten erosion measurements were used to determine each erosion rate.

References

1. A. G. EVANS, in "Treatise on Materials Science and Technology" Vol. 16, edited by C. M. Preece (Academic Press, New York, 1979) pp. 1–67.
2. A. W. RUFF and S. M. WIEDERHORN, *ibid.* pp. 69–126.
3. B. A. LAWN and T. R. WILSHAW, *J. Mater. Sci.* **10** (1975) 1049.
4. M. M. CHAUDHRI and S. M. WALLEY, *Phil. Mag.* **A37** (1978) 153.
5. C. G. KNIGHT, M. V. SWAIN and M. M. CHAUDHRI, *J. Mater. Sci.* **12** (1977) 1573.
6. B. R. LAWN and D. B. MARSHALL, in "Fracture Mechanics of Ceramics" Vol. 3, edited by R. C. Bradt, D. P. H. Hasselman, and F. F. Lange (Plenum Press, New York, 1978) pp. 205–229.
7. B. J. HOCKEY, S. M. WIEDERHORN and H. JOHNSON, *ibid.* pp. 379–402.
8. M. M. CHAUDHRI and P. A. BROPHY, *J. Mater. Sci.* **15** (1980) 345.
9. A. G. EVANS and T. R. WILSHAW, *ibid.* **12** (1977) 97.

10. A. G. EVANS, M. E. GULDEN and M. E. ROSENBLATT, *Proc. Roy. Soc. London Ser.* **A361** (1978) 343.
11. B. J. HOCKEY and B. R. LAWN, *J. Mater. Sci.* **10** (1975) 1275.
12. B. J. HOCKEY and S. M. WIEDERHORN, in "Proceedings of the 5th International Conference on Erosion by Liquid and Solid Impact" (Cavendish Laboratories, University of Cambridge, 1979) pp. 26-1–26-10.
13. B. R. LAWN, B. J. HOCKEY and S. M. WIEDERHORN, *J. Mater. Sci.* **15** (1980) 207.
14. B. R. LAWN and E. R. FULLER, *ibid.* **10** (1975) 2016.
15. S. M. WIEDERHORN and B. R. LAWN, *J. Amer. Ceram. Soc.* **62** (1979) 66.
16. M. E. GULDEN, *ibid.* **64** (1981) C59.
17. M. L. TORTÉ, R. A. ALLIEGRO, D. W. RICHERSON, M. E. WASHBURN and G. Q. WEAVER, *Proc. Brit. Ceram. Soc.* **22** (1973) 125.
18. R. W. RICE, S. W. FREIMAN and P. F. BECKER, *ibid.* **64** (1981) 345.
19. A. G. EVANS and S. M. WIEDERHORN, *J. Mater. Sci.* **9** (1974) 373.
20. W. S. COBLENZ, *J. Amer. Ceram. Soc.* **58** (1975) 530.
21. J. L. CHERMANT, R. MOUSSA and F. OSTERSTOCK, *Rev. Int. Hautes Temp. Réfract.* **18** (1981) 5.
22. J. F. LYNCH, C. G. RUDERER and W. H. DUCKWORTH, "Engineering Properties of Selected Ceramic Materials" (American Ceramic Society, Columbus, Ohio, 1966).
23. L. M. BARKER, in "Fracture Mechanics of Ceramics" Vol. 3, edited by R. C. Bradt, D. P. H. Hasselman and F. F. Lange (Plenum Press, New York, 1978), pp. 483–494.
24. S. M. WIEDERHORN, B. J. HOCKEY and D. E. ROBERTS, *Phil. Mag.* **28** (1973) 783.
25. R. J. JACCODINE, *J. Electrochem. Soc.* **110** (1963) 524.
26. C. ST. JOHN, *Phil. Mag.* **32** (1975) 1193.
27. J. R. HUTCHINS III, and R. V. HARRINGTON, in "Kirk–Othmer Encyclopedia of Chemical Technology", edited by A. Standen (John Wiley and Sons, New York, 1966) pp. 533–604.
28. S. M. WIEDERHORN, *J. Amer. Ceram. Soc.* **52** (1969) 99.
29. J. H. WESTBROOK, *Rev. Hautes Temp. Réfract.* **t. 3** (1966) 47.
30. S. M. WIEDERHORN and D. E. ROBERTS, *Bull. Amer. Ceram. Soc.* **55** (1976) 185.
31. A. W. RUFF and L. K. IVES, *Wear* **35** (1975) 195.
32. R. J. FIELDS Jr, B. J. HOCKEY and S. M. WIEDERHORN, to be published.
33. G. L. SHELDON and I. FINNIE, *J. Eng. Ind., Trans. ASME,* **88** (1966) 393.
34. G. A. SARGENT, P. K. MEHROTRA and H. CONRAD, in "Erosion: Prevention and Useful Applications", ASTM STP 664, edited by W. F. Adler, (American Soceity of Testing and Materials Philadelphia, PA, 1979) pp. 77–100.
35. M. E. GULDEN, *ibid.* pp. 101–122.
36. R. O. SCATTERGOOD and J. L. ROUTBORT, *Wear* **67** (1981) 227.
37. J. L. ROUTBORT, R. O. SCATTERGOOD and P. A. L. TURNER, *ibid.* **59** (1980) 363.
38. J. L. ROUTBORT and R. O. SCATTERGOOD, *J. Amer. Ceram. Soc.* **63** (1980) 593.
39. P. W. BRIDGMAN, "Dimensional Analaysis", (Yale University Press, New Haven, Conn., 1922).
40. B. R. LAWN, A. G. EVANS and D. B. MARSHALL, *J. Amer. Ceram. Soc.* **63** (1980) 574.
41. O. L. DAVIES, "Statistical Methods in Research and Production", (Oliver and Boyd, London, 1957).
42. A. G. ATKINS, in "The Science of Hardness Testing and its Research Applications", edited by J. H. Westbrook and H. Conrad (American Society for Metals, Metals Park, Ohio, 1973) pp. 223–240.
43. T. N. LOLADGE, G. V. BOKUCHAVA and G. E. DAVIDOVA, *ibid.* pp. 251–257.
44. M. G. MENDIRATTA, J. WIMMER and J. BRANSKY, *J. Mater. Sci.* **12** (1977) 212.
45. S. T. GONAZY and D. L. JOHNSON, in "Fracture Mechanics of Ceramics" Vol. 3, edited by R. C. Bradt, D. P. H. Hasselman and F. F. Lange, (Plenum Press, New York, 1978) pp. 495–506.
46. S. M. WIEDERHORN and B. J. HOCKEY, *J. Noncryst. Solids* **38** and **39** (1980) 433.
47. H. P. KIRCHNER and R. M. GRUVER, in "Fracture Mechanics of ceramics", Vol. 3, edited by R. C. Bradt, D. P. H. Hasselman and F. F. Lange (Plenum Press, New York, 1978) pp. 365–377.
48. J. M. KAY and R. M. NEDDERMAN, "An Introduction to Fluid Mechanics and Heat Transfer", 3rd edn (Cambridge University Press, Cambridge, 1974).

Received 18 March
and accepted 19 July 1982